

Article

Activation of the Cyano Group at Imidazole via Copper Stimulated Alcoholysis

Rezeda Gayfullina [†], Sirpa Jääskeläinen, Igor O. Koshevoy and Pipsa Hirva ^{*}

Department of Chemistry, University of Eastern Finland, P.O. Box 111, FI-80101 Joensuu, Finland

^{*} Correspondence: pipsa.hirva@uef.fi[†] Current address: Department of Chemistry, University of Jyväskylä, P.O. Box 35, FI-40014 Jyväskylä, Finland.

Received: 19 June 2019; Accepted: 5 July 2019; Published: 9 July 2019



Abstract: Reactions of 4,5-dicyano-1-methylimidazole with CuX_2 ($\text{X} = \text{Cl}, \text{Br}$) in alcohol solvents (ethanol and methanol) resulted in the formation of Cu(II) carboximidate complexes $[\text{CuCl}_2(5\text{-cyano-4-C(OEt)N-1-methylimidazole})(\text{EtOH})]$ (**1**), $[\text{Cu}_2(\mu\text{-Cl})_2\text{Cl}_2(5\text{-cyano-4-C(OMe)N-1-methylimidazole})_2]$ (**2**), $[\text{Cu}_2(\mu\text{-Br})_2\text{Br}_2(5\text{-cyano-4-C(OMe)N-1-methylimidazole})_2]$ (**3**), and $[\text{Cu}_2(\mu\text{-Br})_2\text{Br}_2(5\text{-cyano-4-C(OEt)N-1-methylimidazole})_2]$ (**4**). The structures were determined by the X-ray crystallographic method, and further spectroscopic and computational methods were employed to explain the structural features. The solvent contributed to the alcoholysis reaction of the cyano group, as the result of which the ligand coordinated to the metal center in bidentate mode forming a five-membered chelating ring. In **1**, the solvent also acts as an additional ligand, which coordinates to the metal center of a monomeric complex. In compounds **2–4**, two halogen ligands link the metal atoms forming dihalo-bridged copper dimers. The infrared absorption characteristics were verified by simulation of the infrared spectra at the density functional theory level. In addition, the electronic absorption characteristics were explained by simulation of the UV–Vis spectra using the TD-DFT method. Molecular modelling at the DFT level was performed to study the effects of halogen type and steric hindrance of the alkoxy groups in forming the copper(II) complexes.

Keywords: copper complex; imidazole; cyano; alcoholysis; structural analysis; DFT; QTAIM (Quantum Theory of Atoms in Molecules)

1. Introduction

Compounds with imidazole rings have been increasingly studied because imidazole plays a significant role in biological processes [1–4]. For instance, some derivatives are used for the treatment of fungal and cancer diseases [5,6]. Imidazoles are found in many medicines, such as antifungal drug series, the sedative midazolam, and the nitroimidazole series of antibiotics [7–10]. On the other hand, imidazole derivatives are used in the synthesis of polymers [11,12] or copolymers [13,14]. Their utilization as ligands with electron acceptor properties and as promising ligands for the synthesis of anisotropic conductors has been reported [15–18].

It is well known, that the CN group is sensitive to nucleophilic attack [19]. Alcoholysis of the nitrile group gives rise to carboximidates or more generally, imidates. The carboximidate group is thus an imino ether and can also be considered as an iminoester formed from carboximide acid and alcohol. Metal complexes with cyanoimidazole ligands are rare. Rasmussen et al. reported synthesis and characterization of the Cu(I) complex, where the 4,5-dicyanoimidazole ligand coordinated to the Cu(I) ion in bidentate fashion via one imidazole N atom and the N atom of the imidato group, which was formed due to a nucleophilic reaction of methanol to one CN group in the presence of carbon monoxide. Typically, imidazole was deprotonated and acted as an anionic ligand. Two triphenylphosphine groups

completed the coordination sphere of the metal [20]. In some Cu(II) complexes based on cyanopyridine ligands, similar alcoholysis of cyano groups takes place [20–26]. The methyl group at the nitrogen atom prevents deprotonation of the imidazole ring in 4,5-dicyano-1-methylimidazole, which is thus less acidic than 4,5-dicyanoimidazole [27]. Therefore, the apparent coordination sites are one of the imidazole nitrogens and the two cyano groups.

Our earlier studies on this ligand in Ag(I) complexes revealed that the polydentate character of 4,5-dicyano-1-methylimidazole gives rise to formation of coordination polymers. In $[\text{Ag}(\text{4,5-dicyano-1-methylimidazole})_2]_n[\text{CF}_3\text{SO}_3]_n$ and $[\text{Ag}_2(\text{4,5-dicyano-1-methylimidazole})_2][\text{NO}_3]_2$, the imidazole N atom and N atom of one cyano group are involved in coordination with Ag(I) ions, whereas in the $[\text{Ag}_2(\text{4,5-dicyano-1-methylimidazole})_2]_n[\text{ClO}_3]_{2n}$ complex, all three coordination sites of the ligand are utilized [28].

There are still no known organometallic complexes derived from 4,5-dicyano-1-methylimidazole, where the ligand coordinates to the metal ion in bidentate fashion through the N atoms of the heterocycle and of carboximidate, obtained from CN activation. However, based on reported carboximidate metal complexes derived from cyanopyridine [20–26] and 4,5-dicyanoimidazole [20], it is logical to assume that such complexes also can be synthesized based on this ligand. Therefore, in the present study, the reactions of 4,5-dicyano-1-methylimidazole with CuCl_2 and CuBr_2 were compared in different alcoholic media. As products, we describe four new Cu(II) complexes based on 4,5-dicyano-1-methylimidazole ligands. All compounds are water soluble, which is typical for imidazole derivatives and broadens the scope of their applicability.

2. Results and Discussion

The Cu(II) complexes 1–4 were synthesized via reactions of CuCl_2 or CuBr_2 with 4,5-dicyano-1-methylimidazole in alcoholic media and successive crystallization at +5 °C. The summary of the reactions is presented in Figure 1.

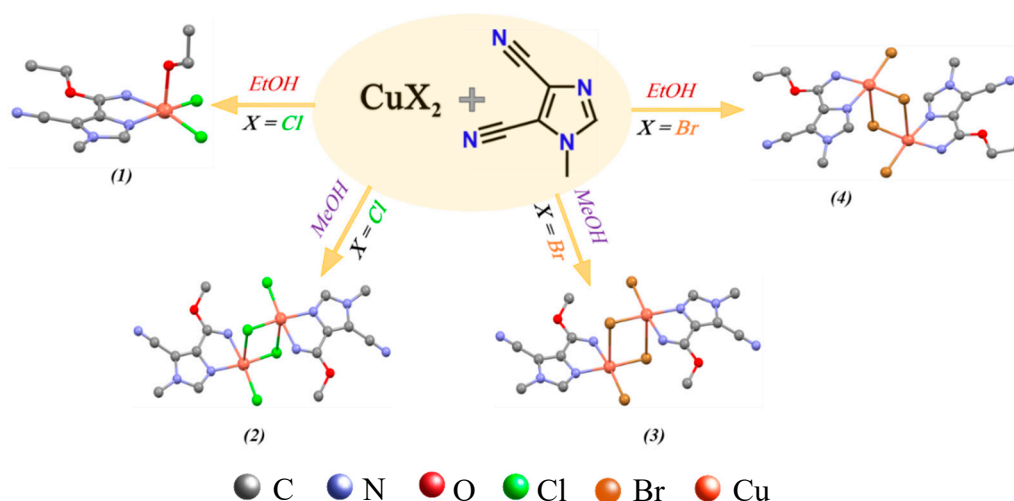


Figure 1. Formation of complexes 1–4. The hydrogen atoms are omitted for clarity.

2.1. Structural Analysis

All the structures were solved by the single-crystal X-ray crystallographic method. X-ray structures for 1–4 are presented in Figure 2 and their important geometric parameters are shown in Table 1. All complexes crystallized in the triclinic crystal system $P\bar{1}$ space group. Complex 1 has a monomeric structure while the others have a centrosymmetric dimeric structure. In 1, the metal center adopts a distorted square-pyramidal geometry with the oxygen atom of coordinated ethanol molecule in the apical position. The binuclear complexes 2–4 adopt the same geometry around the metal center, but they contain a bridging halogen ligand in an apex of the square-pyramid instead of the ethanol

molecule. In all complexes, the square base is completed by two halogen ligands and two nitrogen atoms of the ligand.

The geometries and the ground state spin states of complexes 1–4 were also optimized computationally at the DFT level of theory. The singlet ground state of complex 1 showed a good match with experimental geometry. Furthermore, the optimized geometry of the dimeric complexes 2–4 in the triplet ground state demonstrated good agreement with experimental structures (less than 3% average deviation). The selected optimized parameters are compared with the experimental ones in Tables S1–S4. In addition, the calculations confirmed the presence of the H atom at the imino group in all complexes, and therefore allowed the tautomeric form of the ligand in coordination to be verified.

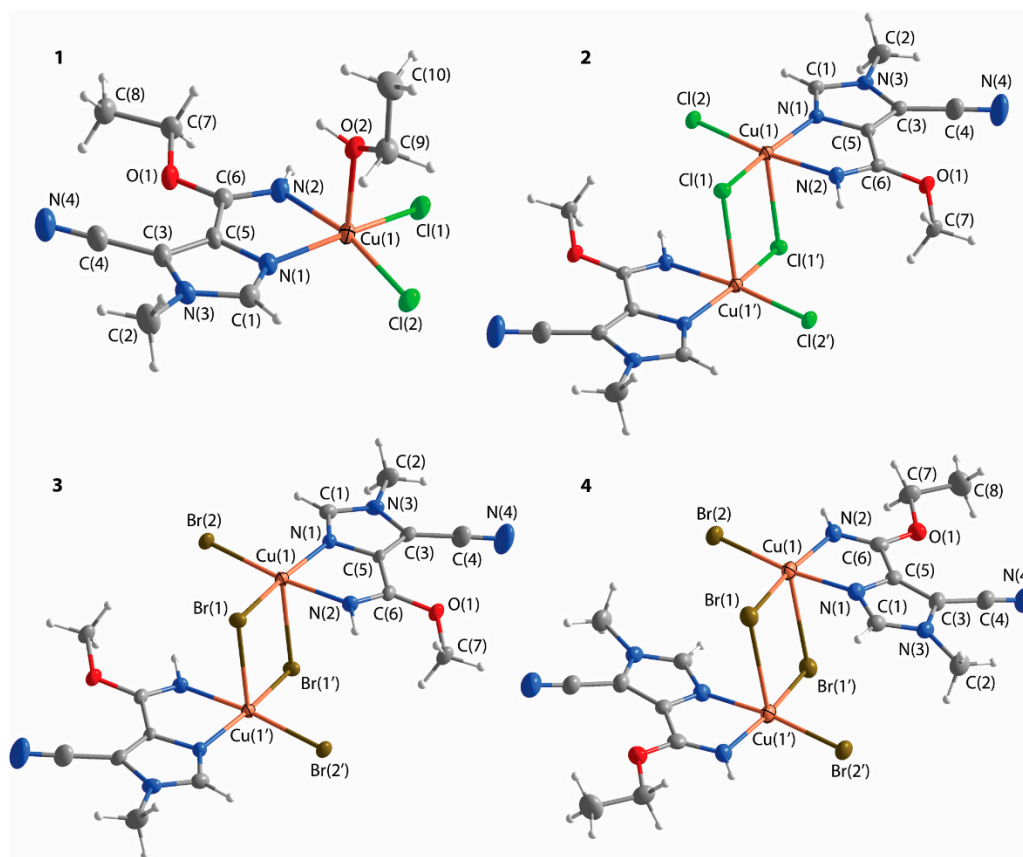


Figure 2. X-ray structures of $[\text{CuCl}_2(5\text{-cyano-4-C(OEt)N-1-methylimidazole})(\text{EtOH})]$ (1), $[\text{Cu}_2(\mu\text{-Cl})_2\text{Cl}_2(5\text{-cyano-4-C(OMe)N-1-methylimidazole})_2]$ (2), $[\text{Cu}_2(\mu\text{-Br})_2\text{Br}_2(5\text{-cyano-4-C(OMe)N-1-methylimidazole})_2]$ (3), and $[\text{Cu}_2(\mu\text{-Br})_2\text{Br}_2(5\text{-cyano-4-C(OEt)N-1-methylimidazole})_2]$ (4). Thermal ellipsoids are shown at 50% probability level.

In the synthesis of the compounds, the presence of alcohol solvent is responsible for the transformation of the ligand. One of the cyano groups undergoes nucleophilic addition of the solvent molecule to generate a chelating imidate ligand. Furthermore, the nature and the oxidation state, and hence the Lewis acidity of the metal plays an important role in the reaction. The earlier reported Ag(I) complexes with 4,5-dicyano-1-methylimidazole showed that the ligand was not susceptible to nucleophilic attack by alcohol solvent [28]. In the copper(II) compounds obtained in the present study, the solvent molecules play an additional role in coordination of the ligands to the metal center. According to computational analysis, the bridging halogens are able to stabilize the dimeric structure in 2–4, but not in 1. One plausible explanation of this behavior is that due to either larger Cu–Br distances of the halogen bridges (optimized distances 2.903 Å vs. 2.789 Å in 4 and 2, respectively), or the smaller size of the solvent molecule (methanol vs. ethanol in 2 and 1, respectively), energetic reasons favor

formation of a dimer in 2–4, but the larger steric demands of the EtOH solvent molecule favor the formation of a monomer in 1. Copper(II) acts as promoter for alcoholysis of the cyano group in the ligand. The solvent not only participates in solvolysis but it also acts as an additional ligand in complex 1. Therefore, copper stimulates the cyano group for alcoholysis reaction, which agrees with previously reported studies [19,30].

Table 1. Important geometry parameters for complexes 1–4.

Parameter	Complex 1	Complex 2	Complex 3	Complex 4
Bond distance (Å)				
Cu1–N1	2.024	2.016	2.016	1.989
Cu1–N2	2.038	2.010	2.012	2.032
Cu1–O2/X' (ax)	2.275	2.781	2.944	3.139
Cu1–X1	2.265	2.250	2.380	2.395
Cu1–X2	2.252	2.250	2.388	2.387
Cu1–Cu1'	-	3.395	3.526	3.860
Angle (°)				
O2/X'–Cu1–X1	100.4	95.8	97.8	92.6
O2/X'–Cu1–X2	97.1	100.7	99.7	105.6
O2/X'–Cu1–N1	91.0	89.8	88.2	78.8
O2/X'–Cu1–N2	92.2	82.5	83.0	88.7
X1–Cu1–N2	89.8	89.9	90.3	170.0
X1–Cu1–N1	165.2	167.9	168.2	90.3
X1–Cu1–X2	96.4	95.8	95.2	95.8
X2–Cu1–N1	91.5	93.7	93.8	172.3
X2–Cu1–N2	167.7	173.1	173.4	93.3
N1–Cu1–N2	80.3	80.2	80.3	80.3
Cu1–N1–C5–C3	–173.6	173.9	–172.8	–168.2
τ **	0.042	0.087	0.085	0.038

** Geometry index $\tau = (\beta - \alpha)/60^\circ$, where $0 \leq \tau \leq 1$, α and β are two largest angles ($\beta > \alpha$); $\tau = 0$ for an ideal square-pyramid, $\tau = 1$ for an ideal trigonal-bipyramid [29].

The ligand coordinates to the metal center through the imidazole nitrogen N1 and the imidato nitrogen N2 to form a five-membered chelating ring in the equatorial position. The Cu1–N1 and Cu1–N2 bond lengths lie in the narrow ranges of 1.989–2.025 Å and 2.009–2.036 Å, respectively, which agree with earlier reported copper(II) complexes [20,21,23,25,31–35]. The nitrogen–halogen distances at basal planes are almost symmetrical in all compounds. The axial bond lengths of Cu1–X' and Cu1–O2 lie in a similar range to earlier published values [36–44]. As expected, the bond distances between the metal center and halogen atoms in the equatorial position are shorter than in the apical position.

Two equatorial angles O2/X'–Cu1–N1 and O2/X'–Cu1–N2 are formed with almost ideal values of 90° , whereas X1–Cu1–X2 is slightly larger than 90° . The bite angle N1–Cu1–N2 is thus less 90° , which is common for this type of coordination [20,21,23,25,31,34] and the apex of the pyramid is slightly shifted towards the two nitrogen atoms. In five-coordinated complexes, the degree of distortion was evaluated by the geometry index τ depending on the two largest angles ($\beta > \alpha$) around the metal center as $\tau = (\beta - \alpha)/60^\circ$, where the τ value varies from 0 to 1.37. The extreme τ values such as 0 and 1 indicate ideal square pyramidal and trigonal-bipyramidal geometries, respectively. The τ value for 1–4 (0.038–0.087) is a sign that almost perfect square pyramidal geometry is formed around the Cu(II) ion. In all complexes, the torsion angle Cu1–N1–C5–C3 is close to 180° , showing that the copper atom is almost co-planar with the imidazole ring.

In the middle of the dimers 2–4, two halogen ligands bridge the copper centers building up a planar Cu_2X_2 unit. The distance between the two copper centers varies between 3.395–3.860 Å, which is typical for dihalo-bridged copper dimers [29,30] and shows no metallophilic interaction between the two copper(II) ions. It is also noteworthy, that in 1–3 the alkoxy group at copper lies in the *trans* position to the terminal halogen, while in 4 it is *trans* to the bridging halogen.

2.2. Computational Studies

We optimized the geometry of the molecular complexes **1–4** in order to compare the nature of the intramolecular interactions and their effect on the structural features by DFT calculations and by performing QTAIM (Quantum Theory of Atoms in Molecules) analysis for the optimized compounds. Figure 3 displays the bond paths and the corresponding bond critical points for the dimeric complexes **2–4**. The results for the analysis are presented in Table 2.

Table 2. Properties of the electron density in the selected bond critical points (BCPs) for compounds **1–4**. For the numbering scheme of the BCPs, see Figure 3. Atom numbers follow the scheme in Figure 2.

BCP#	Type	$\rho(\text{e}\text{\AA}^{-3})$	$ V /G$	$E_{\text{INT}}(\text{kJ}\cdot\text{mol}^{-1})$
<i>[CuCl₂(5-cyano-4-C(OEt)N-1-methylimidazole)(EtOH)] (1)</i>				
1	Cu1–N2	0.496	1.20	–144
2	Cu1–N1	0.473	1.18	–138
3	Cu1–Cl1	0.546	1.34	–136
4'	Cu1–O2	0.206	0.97	–41
5	Cu1–Cl2	0.493	1.31	–119
<i>[Cu₂(μ-Cl)₂Cl₂(5-cyano-4-C(OMe)N-1-methylimidazole)₂] (2)</i>				
1	Cu1–N2	0.525	1.22	–153
2	Cu1–N1	0.505	1.20	–150
3	Cu1–Cl1	0.494	1.31	–121
4	Cu1–Cl1'	0.162	0.99	–25
5	Cu1–Cl2	0.497	1.31	–121
<i>[Cu₂(μ-Br)₂Br₂(5-cyano-4-C(OMe)N-1-methylimidazole)₂] (3)</i>				
1	Cu1–N2	0.525	1.22	–153
2	Cu1–N1	0.491	1.20	–144
3	Cu1–Br1	0.434	1.34	–90
4	Cu1–Br1'	0.160	1.03	–23
5	Cu1–Br2	0.440	1.36	–91
<i>[Cu₂(μ-Br)₂Br₂(5-cyano-4-C(OEt)N-1-methylimidazole)₂] (4)</i>				
1	Cu1–N2	0.526	1.22	–155
2	Cu1–N1	0.496	1.20	–144
3	Cu1–Br2	0.428	1.34	–89
4	Cu1–Br1'	0.144	1.01	–20
5	Cu1–Br1	0.440	1.35	–91

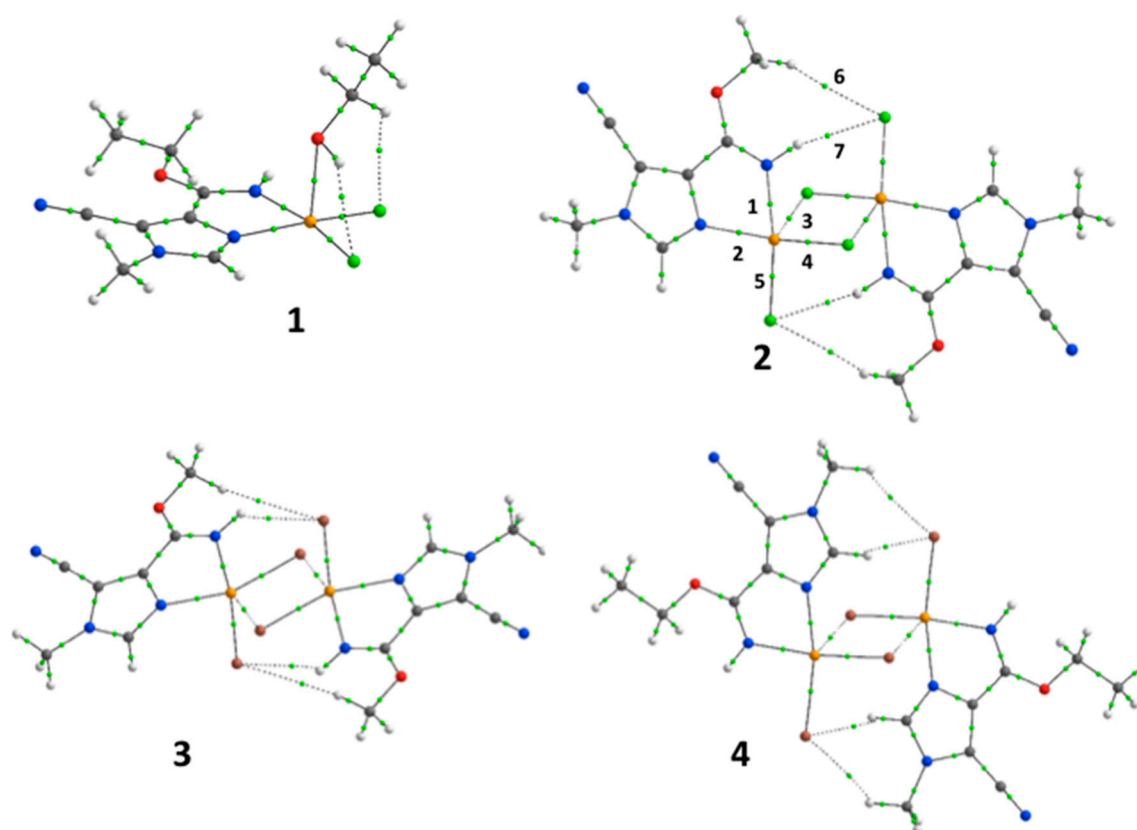


Figure 3. Bond paths and bond critical points (BCPs) in the copper compounds 1–4 according to QTAIM (Quantum Theory of Atoms in Molecules) analysis. Compound 2 shows the numbering of the BCPs, which is used in Table 3 for all compounds. For the color scheme of the atoms, see Figure 1.

The major difference between monomeric compound 1 and dimeric compound 2 is that in the former compound the apical position occupies a solvent molecule instead of a Cl ligand. This is energetically favorable, since the interaction strength of the Cu–O bond in 1 (BCP #4') is about twice the value of the corresponding Cu–Cl in 2 (BCP #4). However, as previously pointed out, there is a subtle balance between electronic and steric effects in complexation.

In dimeric compounds 2–4, the halogen atoms, which are *trans* to nitrogen atoms, coordinate with stronger, partially covalent Cu–X bonds, as can be seen by the larger E_{INT} values and $|V|/G > 1$ for BCPs #3 and #5. The *trans* effect makes a large contribution, therefore there is no difference between the interaction strengths of bridging and non-bridging halogens. On the other hand, the halogen, which has no *trans* atoms in the coordination sphere, shows a rather weak and effectively non-covalent interaction to the copper center (for example, $E_{\text{INT}} = -121 \text{ kJ}\cdot\text{mol}^{-1}$ vs. $-25 \text{ kJ}\cdot\text{mol}^{-1}$ for Cu–Cl). The halogen effect is smaller, Cu–Cl bonds ($E_{\text{INT}} = -121 \text{ kJ}\cdot\text{mol}^{-1}$) are stronger than Cu–Br ($E_{\text{INT}} = -90 \text{ kJ}\cdot\text{mol}^{-1}$). Furthermore, the coordinated nitrogen atom from the activated cyano group forms a slightly stronger interaction with copper than the imidazole nitrogen. Otherwise there are no major differences between the intermolecular interactions in compounds 2–4. Even the intramolecular weak interactions are very similar, and the different orientation of the ligands in 4 vs. 3 has no major effect.

In the solid state of the molecular complexes, several weak intermolecular interactions are present (Figure 4). In 1, intermolecular Cl1–H contact 2.627 \AA to imine hydrogen and N–H contact 2.508 \AA between the free cyano group and the methyl group at the imidazole give rise to a chain structure. Furthermore, Cl1 has a short contact 2.294 \AA to the OH hydrogen at the coordinated ethanol molecule creating a 3D structure. The sum of the van der Waals radii is 2.95 \AA for Cl–H and 2.75 \AA for N–H. In 2 and 3, the nitrogen atom in the uncoordinated cyano group has distances of 2.504 and 2.499 \AA with the H in the methoxy group. In these, the imidazole hydrogen also has short contact with the terminal

halogen of 2.640 Å and 2.757 Å (sum of vdW 3.05 Å for H and Br). In **4** the nitrogen of the free CN forms an interaction of 2.384 Å with the H at the imidazole methyl. The Br⋯H of the imine is 2.788 Å.

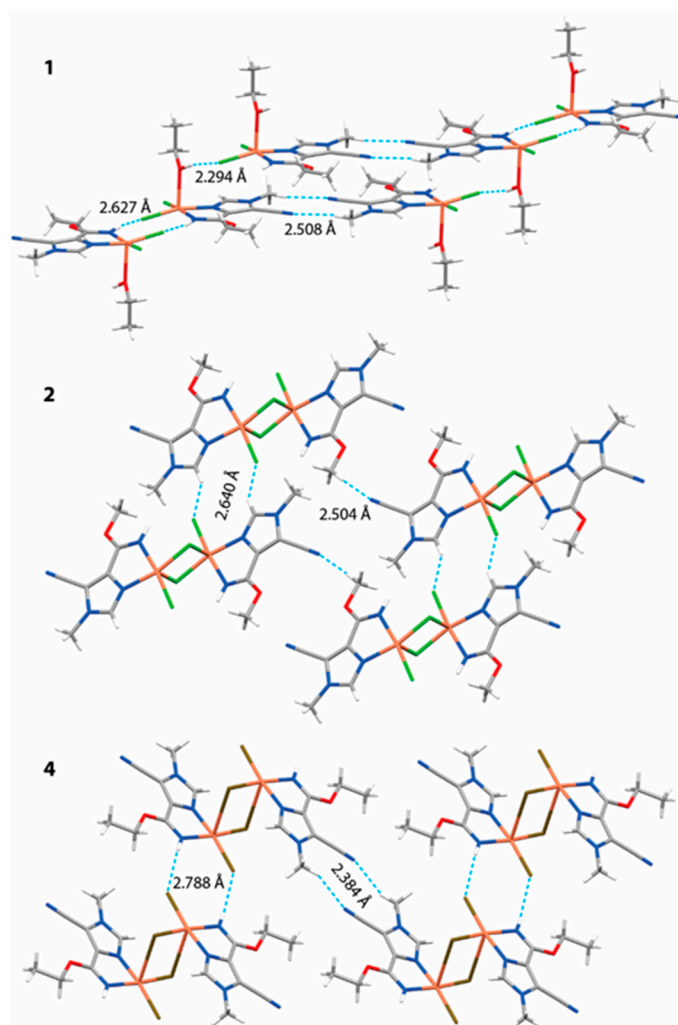


Figure 4. Packing in solid state for **1**, **2**, and **4**. **2** and **3** have a similar type of packing.

The intermolecular interactions were further studied via topological charge density analysis using extended models cut from the crystal structures of **1**, **2**, and **4**. The bond paths and the bond critical points for models (**1**)₄, (**2**)₂, and (**4**)₂ are shown in Figures S1–S3 (See Supplementary Materials). Table S6 lists the properties of the electron density at selected BCPs representing different types of weak intermolecular interactions.

It is no surprise, that the strongest intermolecular interactions are the hydrogen bonds between the chloride ligands and the hydrogen atoms from the OH or NH groups of neighboring molecules. The fairly strong Cl⋯H(O) interactions, compared to compounds **2–4**, further stabilize the crystal structure of **1**. According to the small $|V|/G$ value (<1), all intermolecular interactions are clearly electrostatic in nature. Formation of dimers, however, limits the amount of “free” chlorides (non-bridging), and therefore hydrogen bonding interactions form between the non-modified cyano groups and the MeO/MeN groups.

2.3. IR Analysis

The IR spectra were measured in KBr. The assigned characteristic IR bands for complexes **1–4** agree with the X-ray crystallographic study of the single crystal. The spectra of the complexes significantly differ from the IR spectrum of the free ligand due to the alcoholysis of the cyano group. Table 3 shows

the comparison of the main IR bands of the complexes **1–4** with the free 4,5-dicyano-1-methylimidazole ligand. The infrared absorption characteristics were verified by simulation of the infrared spectra at the density functional theory level. Results for the experimental and computational IR frequencies are given in the supporting information (Tables S7–S11).

Table 3. The most important IR absorptions.

	$\nu(\text{N2-H})$	$\nu(\text{C1-H})$	$\nu(\text{C}\equiv\text{N})$	$\nu(\text{C6}=\text{N2})$	$\nu(\text{C5}=\text{C3})$	$\nu(\text{C-O})$	$\nu_{\text{as}}(\text{C-O})$
				$\nu(\text{C5}=\text{C3})$	$\nu(\text{C6}=\text{N2})$	$\beta(\text{N2-H})$ $\beta(\text{C1-H})$ $\nu(\text{C5-N1})$ $\nu(\text{N3-C2})$	$\rho(\text{Me})/\text{OEt}$ skeletal
	-	3126	2240(vs)	-	-	1316(m) *	-
1	3283	3123	2236(w)	1644(s)	1587(vs)	1304(s)	1007
2	3359	3100	2242(w)	1653(vs)	1593(s)	1298(s)	1145
3	3347	3097	2242(w)	1651(vs)	1591(s)	1296(s)	1144
4	3289	3153	2245(w)	1639(s)	1586(vs)	1302(s)	1005

* there is no $\nu(\text{C-O})$.

The appearance of N2–H stretching at 3359–3283 cm^{-1} and strong C6=N2 stretching bands at 1653–1639 confirm the formation of carboximidate complexes. The intensity of the N2–H stretching bands varies from medium (in **2** and **3**) to weak (in **1**, **4**). The C6=N2 and C5=C3 stretching modes are presented as two sharp intense bands, which are consistent with the previously reported values of the bands [26,45,46].

The modified part of the ligand in the complexes can be considered as an ester including the alkoxy group and the imine group. As a rule, an ester is characterized by two bands of asymmetric C–O stretching in the 1300–1000 cm^{-1} region [47], which in the metal complexes is shifted to higher frequency region [24,30,44]. In all spectra of the complexes **1–4**, a strong band at ca. 1300 cm^{-1} is assigned to the asymmetric C–O stretching mode. The second asymmetric C–O stretching band related to the alkoxy group should lie in the 1200–1000 cm^{-1} region. In **2** and **3**, the band at 1145 and 1144 cm^{-1} , respectively, is attributed to asymmetric C–O stretching combined with the methyl-rocking mode of the methoxy group, which is consistent with earlier reported values of the bands. In **1** and **4**, the asymmetric C–O stretching mode mixed with the skeletal vibrations of ethoxy was observed at 1007 and 1005 cm^{-1} , respectively, which agrees with asymmetric C–O stretching for primary alcohols [48].

The C \equiv N stretching vibration in the complexes appears at almost the same wavenumber as in the free ligand, but the intensity significantly changes from strong to weak. This indicates the decrease of the number of free cyano groups in a molecule. The slight deviation in wavenumbers is probably due to weak intermolecular C \equiv N \cdots H interactions [19].

In the spectrum of **1**, the O–H stretching is observed at 3368 cm^{-1} , which is consistent with the reported value in the literature for organometallic compounds having a coordinated alcohol molecule to the metal atom.

2.4. UV–Vis Analysis

We measured the UV–Vis spectra of compounds **1–4** and analyzed their absorption characteristics via TD-DFT calculations. The experimental and computational results in acetonitrile solution are compared in Table 4, and the selected spectra are shown in Figures S4–S6. It should be noted that because of the many nearly degenerate MOs, the interpretation is complicated by the mixing of several weaker transitions in the excited states. Examples of the MOs involved in the main excitations are presented in Figures S7–S10.

Table 4. The main excitations (λ_{\max} [nm] and type) according to the TD-DFT calculations for compounds **1–4** in acetonitrile. The experimental λ_{\max} values are given in parenthesis.

1		2		3		4	
731 (742)	dd+M(X)LCT	802 (807)	dd+Cl(p)+CN(π)	683 (698)	dd+LM(X)CT	722 (687)	dd+LM(X)CT
399 (380)	dd+Cl(p)+CN(π)	406 (380)	dd+Cl(p)+CN(π)	511 (483)	dd+Br(p)+CN(π)	499 (483)	dd+Br(p)+CN(π)
				315 (303)	dd+LM(X)CT	314 (303)	dd+LM(X)CT
255 (256)	LM(X)CT	255 (255)	LM(X)CT	275 (259)	M(X)LCT+LL	269 (259)	M(X)LCT+LL

Mixing of the different kinds of electronic transitions with excitations between the copper d-orbitals explains the relatively dark color of the crystals. According to the appearance of the MOs shown in Figures S7 and S8, the main difference between the monomeric **1** and dimeric **2** can be seen in the lowest energy signal at 731 nm (**1**) or 802 nm (**2**). In **2**, the lowest energy excitation involves MOs which are concentrated on the Cu- μ (Cl₂)-Cu system, including also some contribution from the π system of the activated cyano group. On the other hand, the lowest energy signal in **1** includes mixing of dd excitation with metal-to-ligand charge transfer, where the ligand part includes also the axial ethanol solvent molecule. This M(X)LCT contribution leads to a blue shift in the lowest energy signal. The other main excitations presented in Table 4 are very similar for both **1** and **2**, and consist mainly of ligand-to-metal-to-halogen charge transfer transitions.

The influence of the halogen is clearly seen in the UV–Vis spectra of bromide-bridged **3** and **4**, when compared with the corresponding chloride compound **2**. The lowest energy excitations are strongly blue-shifted in **3** and **4** because of the larger contribution of the aromatic ligands (Figures S9 and S10). In contrast, the large participation of all the bromide ligands in the excitations at around 500 nm leads to a red-shift compared to the corresponding excitations in **2** (406 nm). Additionally, the signal at 315 nm corresponding to transitions between ligand based orbitals and metal + halogen orbitals is clearly visible only in **3** and **4**. The most intense signals in the UV-area are also red-shifted for **3** and **4**, compared to **2**. The reason for the shift is again the larger halogen-effect of bromido ligands compared to chlorido ligands. However, it can be concluded, that a different solvent (ethanol/methanol) does not present any apparent changes in the electronic excitations.

3. Materials and Methods

3.1. General

Commercially available reagents anhydrous CuCl₂ (99%, Aldrich, St. Louis, MO, USA), CuBr₂ (99%, Aldrich) and 4,5-dicyano-1-methylimidazole (97%, Alfa Aesar, Ward Hill, MA, USA) were used without purification. The organic solvents were dried using molecular sieves. Infrared spectra were measured from KBr pellets using a Bruker VERTEX 70 FT-IR spectrometer (Billerica, MA, USA) in the range of 4000–400 cm⁻¹. The elemental analysis was performed on a varioMICRO V1.7 (Elementar Analysensysteme GmbH, Langenselbold, Germany). The ¹H NMR spectra were recorded in DMSO-d₆ on a Bruker Avance 400 MHz (Bruker Spectrospin, Rheinstetten, Germany). UV–Vis spectra were obtained by a Perkin Elmer Lambda 9000 UV/VIS/NIR spectrometer (Waltham, MA, USA).

3.2. Synthesis of Complexes **1–4**

[CuCl₂(5-cyano-4-C(OEt)N-1-methylimidazole)(EtOH)] (**1**). A solution of 4,5-dicyano-1-methylimidazole (0.0200 g, 0.1514 mmol) in ethanol (2 mL) was added to a solution of CuCl₂ (0.0102 g, 0.0757 mmol) in ethanol (1 mL). After an hour stirring, the resulting solution was filtered. The filtrate was kept at 5 °C for slow evaporation. Pale green crystals of a needle shape were formed after a few days. Yield: 0.0190 g, 70%. Anal. Calc. for C₁₀H₁₆CuN₄O₂Cl₂: C, 33.48; H, 4.50; N, 15.62. Found: C, 33.31; H, 4.43; N, 15.73. IR (KBr, cm⁻¹): 3283 (w), 3123 (w), 2236 (w), 1644 (s), 1587 (vs), 1516 (m), 1304 (s), 1173 (m), 1111 (w), 1079 (w), 1049 (w), 1007 (w), 889 (w), 873

(w), 839 (w), 818 (w). $^1\text{H NMR } \delta$: 8.11 (NH, 1H, s), 4.35 (O-CH₂-CH₃, 2H, br), 3.79 (N-CH₃, 3H, s), 1.06 (O-CH₂-CH₃, 3H, t). UV-Vis [λ_{max} , nm]: acetonitrile 380, 750; DMSO 268, 799.

[Cu₂(μ -Cl)₂Cl₂(5-cyano-4-C(OMe)N-1-methylimidazole)₂] (**2**). 4,5-dicyano-1-methylimidazole (0.0200 g, 0.1514 mmol) and CuCl₂ (0.0407 g, 0.3028 mmol) were dissolved in 1.5 mL and 1 mL methanol, respectively. Blue-greenish needle crystals suitable for X-ray diffraction examination were isolated after a few days. Yield: 0.0340 g, 38%. Anal. Calc. for C₁₄H₁₆Cu₂N₈O₂Cl₄: C, 28.16; H, 2.70; N, 18.76. Found: C, 27.97; H, 2.92; N, 18.47. IR (KBr, cm⁻¹): 3353 (m), 3100 (m), 2242 (w), 1653 (vs), 1593 (s), 1514 (m), 1298 (s), 1181 (w), 1145(w), 1041 (w), 812 (m), 777 (m). $^1\text{H NMR } \delta$: 8.37 (NH, 1H, s), 3.78 (N-CH₃, 3H, s), 1.08 (O-CH₃, 3H, s). UV-Vis [λ_{max} , nm]: acetonitrile 380, 734; DMSO 287.

[Cu₂(μ -Br)₂Br₂(5-cyano-4-C(OMe)N-1-methylimidazole)₂] (**3**). The procedure of the synthesis is similar to complex **2**, but it differs in terms of the metal salt. A solution of the ligand (0.0100 g, 0.0757 mmol) in methanol (0.5 mL) was mixed with a solution of CuBr₂ (0.0338 g, 0.1514 mmol) in methanol (1 mL). Dark green crystals of a needle shape were formed. Yield: 0.007 g, 12%. Anal. Calc. for C₁₄H₁₆Cu₂N₈O₂Br₄: C, 21.70; H, 2.08; N, 14.46. Found: C, 21.70; H, 2.17; N, 14.49. IR (KBr, cm⁻¹): 3347 (m), 3097 (m), 2242 (w), 1651 (vs), 1591 (s), 1514 (m), 1296 (s), 1180 (w), 1144(w), 1039 (w), 810(m), 773 (m). $^1\text{H NMR } \delta$: 8.04 (NH, 1H, s), 3.77 (N-CH₃, 3H, s), 1.00 (O-CH₃, 3H, s). UV-Vis [λ_{max} , nm]: acetonitrile 257, 302, 480; DMSO 274.

[Cu₂(μ -Br)₂Br₂(5-cyano-4-C(OEt)N-1-methylimidazole)₂] (**4**). The ligand (0.0200 g) and CuBr₂ (0.0338 g) were dissolved in 1 mL and 0.8 mL ethanol, respectively. Dark green crystals of a needle shape were formed. Yield: 0.0515 g, 42%. Anal. Calc. for C₁₆H₂₀Cu₂N₈O₂Br₄: C, 23.82; H, 2.51; N, 13.89. Found: C, 23.93; H, 2.68; N, 13.95. IR (KBr, cm⁻¹): 3289 (w), 3153 (w), 2245 (w), 1639 (s), 1586 (vs), 1515 (m), 1302 (s), 1171 (m), 1106 (w), 1043 (w), 1005 (w), 821 (w), 802 (w). $^1\text{H NMR } \delta$: 8.10 (NH, H, s), 4.31 (O-CH₂-CH₃, 2H, br), 3.79 (N-CH₃, 3H, s), 1.06 (O-CH₂-CH₃, 3H, t). UV-Vis [λ_{max} , nm]: acetonitrile 256, 301, 481; DMSO 293.

3.3. Crystal Structure Determination

The crystals of **1–4** were immersed in cryo-oil, mounted in a Nylon loop, and measured at a temperature of 150 K. The X-ray diffraction data were collected on Bruker Kappa Apex II Duo and Smart Apex II diffractometers using Mo K α radiation ($\lambda = 0.71073 \text{ \AA}$). The APEX2 [49] program package was used for cell refinements and data reductions. The structures were solved by direct methods using the SHELXS-2014 [50] program with the WinGX [51] graphical user interface. A semi-empirical absorption correction (SADABS) [52] was applied to all data. Structural refinements were carried out using SHELXL-2014 [50].

The N-H imidate hydrogen atoms were located from the difference Fourier map and constrained to ride on their parent atoms, with $U_{\text{iso}} = 1.2 U_{\text{eq}}$ (parent atom). All other hydrogen atoms were positioned geometrically and constrained to ride on their parent atoms, with C-H = 0.95–0.99 Å and $U_{\text{iso}} = 1.2\text{--}1.5 U_{\text{eq}}$ (parent atom). The crystallographic details are summarized in Table 5.

Table 5. Crystal data and structure refinement for 1–4.

	1	2	3	4
Empirical formula	C ₁₀ H ₁₆ Cl ₂ CuN ₄ O ₂	C ₁₄ H ₁₆ Cl ₄ Cu ₂ N ₈ O ₂	C ₁₄ H ₁₆ Br ₄ Cu ₂ N ₈ O ₂	C ₈ H ₁₀ Br ₂ CuN ₄ O
<i>F_w</i> (g·mol ⁻¹)	358.71	597.23	775.07	401.56
Crystal system	Triclinic	Triclinic	Triclinic	Triclinic
Space group	<i>P</i> $\bar{1}$	<i>P</i> $\bar{1}$	<i>P</i> $\bar{1}$	<i>P</i> $\bar{1}$
<i>a</i> (Å)	5.6535(5)	7.1887(4)	7.3978(2)	7.3737(9)
<i>b</i> (Å)	10.3149(8)	7.4368(5)	7.6151(2)	8.4147(11)
<i>c</i> (Å)	13.5498(10)	10.5356(7)	10.7043(3)	10.6554(14)
α (°)	108.336(3)	82.585(3)	81.023(2)	83.614(5)
β (°)	95.921(3)	89.776(3)	88.684(2)	76.079(5)
γ (°)	98.615(3)	84.799(3)	84.835(2)	75.706(5)
<i>Z</i>	2	1	1	2
ρ_{calc} (Mg·m ⁻³)	1.627	1.783	2.170	2.148
μ (Mo K α) (mm ⁻¹)	1.859	2.421	8.556	8.178
<i>F</i> (000)	366	298	370	386
θ range for data collection (°)	1.604 to 29.000	1.949 to 29.999	1.926 to 28.998	1.972 to 26.998
Refl. collected	28668	24042	20109	18426
Independent refl.	3882 [R(int) = 0.0514]	3229 [R(int) = 0.0466]	3143 [R(int) = 0.0703]	2728 [R(int) = 0.0767]
GOOF on <i>F</i> ²	1.023	1.050	1.079	1.024
Final R indices	R1 = 0.0363, <i>w</i> R2 =	R1 = 0.0295, <i>w</i> R2 =	R1 = 0.0546, <i>w</i> R2 =	R1 = 0.0349, <i>w</i> R2 =
[<i>I</i> > 2 σ (<i>I</i>)] ^a	0.0813	0.0707	0.1000	0.0668
R indices (all data)	R1 = 0.0541, <i>w</i> R2 =	R1 = 0.0438, <i>w</i> R2 =	R1 = 0.0724, <i>w</i> R2 =	R1 = 0.0709, <i>w</i> R2 =
	0.0878	0.0753	0.1068	0.0771

$$^a R_1 = \sum |F_o| - |F_c| / \sum |F_o|; wR2 = [\sum [w(F_o^2 - F_c^2)^2] / \sum [w(F_o^2)^2]]^{1/2}.$$

3.4. Computational Details

All calculations were performed by applying Gaussian 09 software package [53]. The optimized geometry and simulated non-scaled infrared spectra for the copper(II) complexes were obtained by PBE0 functional [54] with 6-311+(d) basis set for non-metal atoms and Def2-TZVPPD basis set [31–36] for copper atom.

To obtain the electronic properties of the complexes, we performed topological charge density analysis with the QTAIM (Quantum Theory of Atoms in Molecules) [55] method, which allowed us to access the nature of the bonding via calculating different properties of the electron density at the bond critical points (BCPs). The analysis was done with the AIMALL program [56] using the wavefunctions obtained from the DFT calculations.

TD-DFT calculations were employed to further compare the electronic properties of the complexes. The UV–VIS spectra were simulated with fully optimized separate molecular models. Solvent effects of the acetonitrile solvent were calculated with the conductor-like polarized continuum model (CPCM) [57] for the gas phase optimized structures.

4. Conclusions

In this research, we described four new Cu(II) complexes based on 4,5-dicyano-1-methylimidazole ligands. Both the nature of the metal and the solvent play an important role in the coordination of the ligand to the metal center. Copper (II) acts as the promoter for the alcoholysis of the cyano group in the ligand. This leads to the formation of the carboximidate group thereby transforming the 4,5-dicyano-1-methylimidazole into bidentate chelating ligand. The solvent not only participates in solvolysis but it also acts as a second ligand in complex 1. Both the modification of one of the cyano groups and the coordination of the solvent were verified via detailed analysis of the IR bands, assisted by computational simulation of the spectra.

In addition, molecular modelling at the DFT level of theory was performed to study the effects of the halogen type and the steric hindrance of the alkoxy groups on the formation of the copper(II) complexes. The formation of the monomeric or dimeric complex was found to be determined by very

small differences in the electronic and steric properties of the coordination sphere of copper. On the other hand, the absorption characteristics of the compounds do not depend on the type of solvent or the nuclearity of the complexes because of the rather similar coordination spheres of the Cu(II) ions. Comparison of the experimental and computationally simulated UV–Vis spectra showed that the main source of differences in the excitations is the type of halogen. Bromido ligands were found to have a larger contribution on the molecular orbitals involved in the main excitations, and therefore a larger halogen effect than the chlorido ligands.

Supplementary Materials: The following are available online at <http://www.mdpi.com/2304-6740/7/7/87/s1>. The crystallographic data for compounds [CuCl₂(5-cyano-4-C(OEt)N-1-methylimidazole)(EtOH)] (1), [Cu₂(μ-Cl)₂Cl₂(5-cyano-4-C(OMe)N-1-methylimidazole)₂] (2), [Cu₂(μ-Br)₂Br₂(5-cyano-4-C(OMe)N-1-methylimidazole)₂] (3), and [Cu₂(μ-Br)₂Br₂(5-cyano-4-C(OEt)N-1-methylimidazole)₂] (4) were deposited with the Cambridge Crystallographic Data Centre as supplementary publication no. CCDC 1921767–1921770. Copies of this information may be obtained free of charge via www.ccdc.cam.ac.uk/data_request/cif. Supplementary material includes the cif and checkcif files for 1–4. The experimental and the optimized geometry parameters are also included. Supplementary material includes also the experimental IR data and UV–Vis spectra; data of simulated IR spectra and UV–Vis spectra and the interpretation of the selected excitations, as well as bond paths and bond critical points of extended models of 1–4. Supplementary data associated with this article can be found in the online version.

Author Contributions: Preparation of complexes was performed by R.G.; spectroscopic measurements and analysis were performed by R.G. and S.J. Preparation of the manuscript draft was carried out by R.G. Theoretical calculations and computational analysis were performed by P.H. The project was planned and supervised by S.J. and P.H. Structural analysis was done by R.G. under supervision of I.O.K. The final revision of the manuscript was made by all the authors.

Funding: This research received no external funding.

Acknowledgments: We acknowledge grants of computer capacity from the Finnish Grid and Cloud Infrastructure (persistent identifier urn:nbn:fi:research-infras-2016072533). COST action CM1302: European Network on Smart Inorganic Polymers (SIPs) is also gratefully acknowledged.

Conflicts of Interest: The authors declare no conflict of interest.

References

1. Satterfield, M.; Brodbelt, J.S. Relative Binding Energies of Gas-Phase Pyridyl Ligand/Metal Complexes by Energy-Variable Collisionally Activated Dissociation in a Quadrupole Ion Trap. *Inorg. Chem.* **2001**, *40*, 5393–5400. [[CrossRef](#)] [[PubMed](#)]
2. Wang, Z.-M.; Lin, H.-K.; Zhu, S.-R.; Liu, T.-F.; Chen, Y.-T. Spectroscopy, cytotoxicity and DNA-binding of the lanthanum(III) complex of an l-valine derivative of 1,10-phenanthroline. *J. Inorg. Biochem.* **2002**, *89*, 97–106. [[CrossRef](#)]
3. Masood, M.A.; Hodgson, D.J. Synthesis and characterization of the multidentate ligand 2,9-bis(N-pyrazolylmethyl)-1,10-phenanthroline (bpmp) and its copper(I) and copper(II) complexes. *Inorg. Chem.* **1993**, *32*, 4839–4844. [[CrossRef](#)]
4. Erden, I.; Demirhan, N.; Avciata, U. Synthesis and Characterization of a New Imidazole Ligand and its Complexes with Cobalt(II), Nickel(II) and Copper(II). *Synth. React. Inorg. Met. Nano-Metal. Chem.* **2007**, *36*, 559–562. [[CrossRef](#)]
5. Handyside, T.M.; Lockhart, J.C.; McDonnell, M.B.; Rao, P.V.S. Ligands for the alkali metals. Part 6. Some bis(crown) Schiff bases which form pocket complexes with alkali-metal cations of appropriate size. *J. Chem. Soc. Dalton Trans.* **1982**, 2331–2336. [[CrossRef](#)]
6. Sandbhor, U.; Kulkarni, P.; Padhye, S.; Kundu, G.; MacKenzie, G.; Pritchard, R. Antimelanomal activity of the copper(II) complexes of 1-substituted 5-amino-imidazole ligands against B16F10 mouse melanoma cells. *Bioorg. Med. Chem. Lett.* **2004**, *14*, 2877–2882. [[CrossRef](#)] [[PubMed](#)]
7. Katritzky, A.R.; Rees, C.W. *Comprehensive Heterocyclic Chemistry: The Structure, Reactions, Synthesis, and Uses Of Heterocyclic Compounds*; Pergamon Press: Oxford, UK, 1984.
8. Grimmett, M.R. *Imidazole and Benzimidazole Synthesis*; Academic Press: New York, NY, USA, 1997.
9. Brown, E.G. *Ring Nitrogen and Key Biomolecules: The Biochemistry of N-Heterocycles*; Springer Science + Business Media: Dordrecht, The Netherlands, 1998.

10. Pozharskii, A.F.; Soldatenkov, A.T.; Katritzky, A.R. *Heterocycles in Life and Society: An Introduction to Heterocyclic Chemistry and Biochemistry and the Role of Heterocycles in Science, Technology, Medicine, and Agriculture*; John Wiley & Sons: Chichester, UK, 1997.
11. Li, J.-X.; Du, Z.-X.; Zhou, J.; An, H.-Q.; Zhu, B.-L.; Wang, S.-R.; Zhang, S.-M.; Wu, S.-H.; Huang, W.-P. A potassium and cadmium coordination polymer connected by two kinds of coordination modes of 4,5-dicyanoimidazole ligands: Synthesis, crystal structure and fluorescent properties of $\{[K[Cd(dci)_2(H_2O)_2]_6]Cl\}_n$. *Inorg. Chem. Commun.* **2010**, *13*, 127–130. [[CrossRef](#)]
12. Hu, T.-P.; Wang, X.-X.; Zheng, B.-H.; Wang, X.-Q.; Hao, X.-N.; Liu, J.-F. Assembly of a 3D chiral Cu(I) metal–organic framework based on 4,5-dicyanoimidazole: CD spectrum, luminescence and selective gas adsorption. *Inorg. Chem. Commun.* **2016**, *68*, 17–20. [[CrossRef](#)]
13. Wu, K.; Chang, T.; Wang, Y.; Hong, Y.; Wu, T. Interactions and mobility of copper(II)–Imidazole-containing copolymers. *Eur. Polym. J.* **2003**, *39*, 239–245. [[CrossRef](#)]
14. Carella, A.; Centore, R.; Riccio, P.; Sirigu, A.; Quatela, A.; Palazzesi, C.; Casalboni, M. Polymethacrylate Copolymers Containing 4,5-Dicyanoimidazole-Based Chromophores and their Nonlinear Optical Behavior. *Macromol. Chem. Phys.* **2005**, *206*, 1399–1404. [[CrossRef](#)]
15. Cocco, M.; Olla, C.; Onnis, V.; Schivo, M.; De Logu, A. 1-Acylamonoimidazoles synthesis and antimicrobial activity. *Farmaco* **1992**, *47*, 229–238. [[PubMed](#)]
16. Sundberg, R.J.; Martin, R.B. Interactions of histidine and other imidazole derivatives with transition metal ions in chemical and biological systems. *Chem. Rev.* **1974**, *74*, 471–517. [[CrossRef](#)]
17. Townsend, L.B.; Revankar, G.R. Benzimidazole nucleosides, nucleotides, and related derivatives. *Chem. Rev.* **1970**, *70*, 389–438. [[CrossRef](#)] [[PubMed](#)]
18. Chao, H.; Ye, B.-H.; Li, H.; Li, R.-H.; Zhou, J.-Y.; Ji, L.-N. Synthesis, electrochemical and spectroscopic properties of ruthenium(II) complexes containing 1,3-bis([1,10]phenanthroline-[5,6-d]imidazol-2-yl) benzene. *Polyhedron* **2000**, *19*, 1975–1983. [[CrossRef](#)]
19. Storhoff, B.N.; Lewis, H.C., Jr. Organonitrile complexes of transition metals. *Coord. Chem. Rev.* **1977**, *23*, 1–29. [[CrossRef](#)]
20. Rasmussen, P.; Rongguang, L.; Butler, W.; Bayón, J. Dicyanoimidazole complexes of Cu(I): A carbonyl assisted alcoholysis of nitrile. *Inorg. Chim. Acta* **1986**, *118*, 7–13. [[CrossRef](#)]
21. Du, M.; Zhao, X.-J.; Batten, S.R.; Ribas, J. From 1-D Coordination Polymers to 3-D Hydrogen-Bonding Networks: Crystal Engineering and Magnetism of Cu^{II} -dca-Cyanopyridine Supramolecular Systems (dca = Dicyanamide, $N(CN)_2^-$). *Cryst. Growth Des.* **2005**, *5*, 901–909. [[CrossRef](#)]
22. Du, M.; Wang, Q.; Wang, Y.; Zhao, X.-J.; Ribas, J. Metal dicyanamide layered coordination polymers with cyanopyridine co-ligands: Synthesis, crystal structures and magnetism. *J. Solid State Chem.* **2006**, *179*, 3926–3936. [[CrossRef](#)]
23. Mei, L.; Jia, X.; Cheng, Z.J. Synthesis and catalytic activity of metallo-organic complexes bearing 5-amino 2-ethylpyridine-2-carboximidate. *J. Chem. Sci.* **2016**, *128*, 855–860. [[CrossRef](#)]
24. Devi, R.B.; Devi, S.P.; Singh, R.B.; Singh, R.H.; Swu, T.; Devi, W.R.; Singh, C.B. Synthesis, spectroscopic, and biological studies on copper(II) complexes containing equatorial–apical chloride bridges: Crystal structure of $[Cu_2(\mu-Cl)_2(O-2-butoxyethylpyridine-2-carboximidate)_2Cl_2]$. *J. Coord. Chem.* **2014**, *67*, 891–909. [[CrossRef](#)]
25. Xuan, R.-C.; Xu, M.; Cheng, D.-P. Dichloro (O-ethyl 3-methylpyridine-2-carboximidic acid- κ^2N,N') copper(II). *Acta Crystallogr. Sect. C Cryst. Struct. Commun.* **2006**, *62*, m587–m589. [[CrossRef](#)] [[PubMed](#)]
26. Gurbanov, A.V.; Mahmoudi, G.; Da Silva, M.F.C.G.; Zubkov, F.I.; Mahmudov, K.T.; Pombeiro, A.J. Cyanosilylation of aldehydes catalyzed by mixed ligand copper(II) complexes. *Inorg. Chim. Acta* **2018**, *471*, 130–136. [[CrossRef](#)]
27. Kelley, S.P.; Nuss, J.S.; Rogers, R.D. Nonstoichiometric, Protic Azolium Azolate Ionic Liquids Provide Unique Environments for N-Donor Coordination Chemistry. *Chem. Eur. J.* **2015**, *21*, 17196–17199. [[CrossRef](#)] [[PubMed](#)]
28. Jaaskelainen, S.; Appiah, N.S.; Koshevoy, I.; Hirva, P.; Appiah, N.S.; Koshevoy, I. Impacts of the counter ions on 4,5-dicyano-1-methylimidazole silver coordination. *New J. Chem.* **2018**, *42*, 3363–3370. [[CrossRef](#)]
29. Addison, A.W.; Rao, T.N.; Reedijk, J.; Van Rijn, J.; Verschoor, G.C. Synthesis, structure, and spectroscopic properties of copper (II) compounds containing nitrogen–sulphur donor ligands; the crystal and molecular structure of aqua[1,7-bis(N-methylbenzimidazol-2'-yl)-2,6-dithiaheptane] copper(II) perchlorate. *J. Chem. Soc. Dalton Trans.* **1984**, 1349–1356. [[CrossRef](#)]

30. Jamnický, M.; Segl' A, P.; Koman, M. Methanolysis of pyridine-2-carbonitrile in the coordination sphere of copper(II), cobalt(II) and nickel(II). The structure of $[\text{Ni}(o\text{-methylpyridine-2-carboximidate})_3]\text{Br}_2 \cdot 4\text{H}_2\text{O}$. *Polyhedron* **1995**, *14*, 1837–1847. [[CrossRef](#)]
31. Godlewska, S.; Jezierska, J.; Baranowska, K.; Augustin, E.; Dołęga, A. Copper(II) complexes with substituted imidazole and chlorido ligands: X-ray, UV-Vis, magnetic and EPR studies and chemotherapeutic potential. *Polyhedron* **2013**, *65*, 288–297. [[CrossRef](#)]
32. Sun, Y.; Lemaire, V.; Beltrán, J.I.; Cornil, J.; Huang, J.; Zhu, J.; Wang, Y.; Fröhlich, R.; Wang, H.; Jiang, L.; et al. Neutral Mononuclear Copper(I) Complexes: Synthesis, Crystal Structures, and Photophysical Properties. *Inorg. Chem.* **2016**, *55*, 5845–5852. [[CrossRef](#)]
33. Du, H.; Sivappa, R.; Lovely, C.J.; He, Y. New Methods of Imidazole Functionalization—From Imidazole to Marine Alkaloids. *Synlett* **2006**, *2006*, 965–992. [[CrossRef](#)]
34. Gulli, S.; Poli, R.; Daran, J.-C.; Daran, J. Synthesis and Structure of Four-Coordinate Copper(II) Complexes Stabilized by β -Ketiminato Ligands and Application in the Reverse Atom-Transfer Radical Polymerization of Styrene. *Eur. J. Inorg. Chem.* **2011**, *2011*, 1666–1672. [[CrossRef](#)]
35. Sreekanth, A.; Kurup, M.R.P. Structural and spectral studies on four coordinate copper(II) complexes of 2-benzoylpyridine *N*(4),*N*(4)-(butane-1,4-diyl)thiosemicarbazone. *Polyhedron* **2003**, *22*, 3321–3332. [[CrossRef](#)]
36. Yang, L.; Chen, W.; Chen, Y.; Liu, W.; Lei, T.; Li, L.; Lin, M.; Wu, J.; Cao, Y.; Li, W.; et al. Copper(II) and Cadmium(II) Complexes Based on *N,N*-Bis(3,5-dimethyl-2-hydroxybenzyl)-*N*-(2-pyridylmethyl) amine Ligand: Syntheses, Structures, Magnetic, and Luminescent Properties. *Z. Anorg. Allg. Chem.* **2012**, *638*, 1833–1838. [[CrossRef](#)]
37. O'Connor, C.J.; Eduok, E.E.; Owens, J.W.; Stevens, E.D.; Klein, C.L. The synthesis, magnetic properties, and crystal structure of two copper(II) complexes prepared from 2-aminomethylpyridine. *Inorg. Chim. Acta* **1986**, *117*, 175–181. [[CrossRef](#)]
38. Helis, H.M.; Goodman, W.H.; Wilson, R.B.; Morgan, J.A.; Hodgson, D.J. A novel halogen-bridged system: Synthesis and structures of dibromo [2-(2-aminomethyl) pyridine] copper(II) and dibromo (2-methyl-, 2-diaminopropane) copper(II). *Inorg. Chem.* **1977**, *16*, 2412–2416. [[CrossRef](#)]
39. Žilić, D.; Maity, D.; Cetina, M.; Molčanov, K.; Džolić, Z.; Herak, M. Magnetostructural Characterization of Oxalamide Dihalo-Bridged Copper Dimers: Intra- and Interdimer Interactions Studied by Single-Crystal Electron Spin Resonance Spectroscopy. *ChemPhysChem* **2017**, *18*, 2397–2408. [[CrossRef](#)]
40. Yang, J.-P.; Hu, H.-P.; Cheng, Z.-Y.; Qiu, X.-J.; Wang, C.-X. Structural insights into the coordination and selective extraction of copper(II) by tertiary amine ligands derived from 2-aminomethylpyridine. *Polyhedron* **2017**, *128*, 76–84. [[CrossRef](#)]
41. Gentschev, P.; Möller, N.; Krebs, B. New functional models for catechol oxidases. *Inorg. Chim. Acta* **2000**, *300–302*, 442–452. [[CrossRef](#)]
42. Grigereit, T.E.; Ramakrishna, B.L.; Place, H.; Willett, R.D.; Pellacani, G.C.; Manfredini, T.; Menabue, L.; Bonomartini-Corradi, A.; Battaglia, L.P. Structures and magnetic properties of trinuclear copper(II) halide salts. *Inorg. Chem.* **1987**, *26*, 2235–2243. [[CrossRef](#)]
43. Kapoor, R.; Kataria, A.; Venugopalan, P.; Kapoor, P.; Corbella, M.; Rodríguez, M.; Romero, I.; Llobet, A. New Tetranuclear Cu(II) Complexes: Synthesis, Structure, and Magnetic Properties. *Inorg. Chem.* **2004**, *43*, 6699–6706. [[CrossRef](#)]
44. Macías, B.; Villa, M.V.; Chicote, E.; Martín-Velasco, S.; Castiñeiras, A.; Borrás, J. Copper complexes with dithiocarbamates derived from natural occurring amino acids. Crystal and molecular structure of $[\text{Cu}(\text{en})(\text{EtOH})(\text{H}_2\text{O})_3][\text{Cu}(\text{dtc-pro})_2]$. *Polyhedron* **2002**, *21*, 1899–1904. [[CrossRef](#)]
45. Barnard, B.F.B. Metal-promoted reactions of 2-cyanopyridine: Iron(II), cobalt(II), nickel(II), and copper(II) complexes of *O*-methylpyridine-2-carboximidate. *J. Chem. Soc. A Inorg. Phys. Theor.* **1969**, 2140–2144. [[CrossRef](#)]
46. Cini, R.; Caputo, P.A.; Intini, F.P.; Natile, G. Mechanistic and Stereochemical Investigation of Imino Ethers Formed by Alcoholysis of Coordinated Nitriles: X-ray Crystal Structures of *cis*- and *trans*-Bis(1-imino-1-methoxyethane)dichloroplatinum(II). *Inorg. Chem.* **1995**, *34*, 1130–1137. [[CrossRef](#)]
47. Socrates, G. *Infrared and Raman Characteristic Group Frequencies: Tables and Charts*, 3rd ed.; John Wiley & Sons: Chichester, UK, 2001.
48. Pavia, D.L.; Lapman, G.M.; Kriz, G.S. *Introduction to Spectroscopy*, 3rd ed.; Saunders Golden Sunburst Series; Thomson Brooks/Cole: Belmont, CA, USA, 1996.

49. Bruker AXS. *APEX2—Software Suite for Crystallographic Programs*; Bruker AXS, Inc.: Madison, WI, USA, 2010.
50. Sheldrick, G.M. Crystal structure refinement with SHELXL. *Acta Crystallogr. C: Struct. Chem.* **2015**, *71*, 3–8. [[CrossRef](#)]
51. Farrugia, L.J. WinGX and ORTEP for Windows: An update. *J. Appl. Crystallogr.* **2012**, *45*, 849–854. [[CrossRef](#)]
52. Sheldrick, G.M. *SADABS-2008/1—Bruker AXS Area Detector Scaling and Absorption Correction*; Bruker AXS: Madison, WI, USA, 2008.
53. Frisch, M.J.; Trucks, G.W.; Schlegel, H.B.; Scuseria, G.E.; Robb, M.A.; Cheeseman, J.R.; Scalmani, G.; Barone, V.; Mennucci, B.; Petersson, G.A.; et al. *Gaussian 09, Revision, C.01*; Gaussian, Inc.: Wallingford, CT, USA, 2009.
54. Perdew, J.P.; Ernzerhof, M.; Burke, K. Rationale for mixing exact exchange with density functional approximations. *J. Chem. Phys.* **1996**, *105*, 9982–9985. [[CrossRef](#)]
55. Bader, R.F.W. *Atoms in Molecules: A Quantum Theory*; Oxford University Press: Oxford, UK, 1990.
56. Keith, T.A. *AIMAll (Version 12.06.03), TK Gristmill Software*; AIMAll: Overland Park, KS, USA, 2003.
57. Cossi, M.; Rega, N.; Scalmani, G.; Barone, V. Energies, structures, and electronic properties of molecules in solution with the C-PCM solvation model. *J. Comput. Chem.* **2003**, *24*, 669–681. [[CrossRef](#)]



© 2019 by the authors. Licensee MDPI, Basel, Switzerland. This article is an open access article distributed under the terms and conditions of the Creative Commons Attribution (CC BY) license (<http://creativecommons.org/licenses/by/4.0/>).